Journal of Nuclear Materials 545 (2021) 152688

Contents lists available at ScienceDirect

Journal of Nuclear Materials

journal homepage: www.elsevier.com/locate/jnucmat

In-situ ion irradiation induced grain growth in nanocrystalline ceria

C.J. Ulmer[a,*], W-Y. Chen[b], D.E. Wolfe[c], A.T. Motta[a]

[a] Department of Nuclear Engineering, The Pennsylvania State University, University Park, PA 16802, USA
[b] Nuclear Science and Engineering Division, Argonne National Laboratory, Argonne, IL 60439, USA
[c] Department of Materials Science and Engineering, The Pennsylvania State University, University Park, PA 16802, USA

ARTICLE INFO

Article history:
Received 16 June 2020
Revised 14 November 2020
Accepted 16 November 2020
Available online 30 November 2020

Keywords:
Ceria
Ion irradiation
Grain growth
In-situ
TEM

ABSTRACT

Irradiation grain growth of CeO_2 was studied using in-situ ion irradiation with transmission electron microscopy (TEM). Thin films of ceria were produced by electron beam physical vapor deposition (EB-PVD) and then irradiated at the Intermediate Voltage Electron Microscope (IVEM) with 1 MeV Kr^{2+} ions at temperatures of 400°C, 600°C, and 800°C. During irradiation at the elevated temperatures, the CeO_2 phase remained stable and its grains grew with irradiation. Grain growth was only weakly dependent on irradiation temperature between 400°C and 800°C. The grain growth kinetics were evaluated by a thermal spike model that was used to calculate the activation energy for grain growth.

1. Introduction

Grain size is an important material characteristic that affects mechanical, thermal, and electrical properties. In the nuclear industry, engineered nanocrystalline materials have been studied for their improved radiation resistance, and, for the fuel material UO_2, grain size is of concern as it can affect thermal conductivity and the transport and release of gaseous fission products. CeO_2 can be used as an ersatz nuclear fuel for experiments because it shares the same fluorite crystal structure as UO_2 and has a similar melting temperature [1–6].

When subjected to isothermal annealing, grain size typically increases following a kinetic equation of the form

$$D^n - D_0^n = Kt \tag{1}$$

where D_0 and D are the initial and final average grain diameters, K is a kinetic parameter representing the grain boundary mobility, t is the hold time, and n is a constant. For "normal"[†] grain growth of a single-phase material under a thermal driving force, Hillert [7] showed that $n = 2$, although others report that in practice its value may be higher, up to $n = 3$, corresponding to slower kinetics caused by solute and pore drag [8,9]. Sintering was used to study the grain growth kinetics of ceria and the exponent was found to be $n = 2$ and $n = 3$ for pure ceria [10,11]. Other researchers have observed grain growth in ceria as a result of irradiation. Grain growth in nanocrystalline ceria was observed using X-ray methods after 3 MeV Au ion irradiation experiments [12,13]. In that work it was suggested that grain growth was driven by reactions of irradiation-induced disorder with grain boundaries with $n = 5$ [14]. However, more recently Chang et al. found nanocrystalline ceria grain size decreased after 1.5 MeV Au ion irradiation [15]. The decrease in grain size was attributed to a loss of crystallinity as a result of irradiation.

In this work, the grain growth of nanocrystalline ceria under irradiation was studied. Thin films of ceria were created and then ion irradiated in-situ while examining the sample with transmission electron microscopy (TEM). TEM was used to image the grains in order to measure the changes in grain size caused by irradiation. Irradiations were performed at several temperatures to further investigate the competing effects of irradiation and temperature on grain growth in ceria. Finally, the grain growth kinetics were fit to a thermal spike model of grain growth and evaluated. Results are discussed in terms of existing models.

2. Experiment

2.1. CeO_2 samples

CeO_2 samples were prepared for in-situ TEM grain growth experiments by electron beam physical vapor deposition (EB-PVD) [16]. A Denton vacuum system was used to evaporate a CeO_2 target and deposit directly onto copper and molybdenum TEM grids

* Corresponding author. 205 Hallowell Bldg, Atherton Street, University Park, PA 16802
E-mail address: chris@cjulmer.com (C.J. Ulmer).

[†] By "normal" grain growth it is meant a process in which no one grain grows much more than the others.

https://doi.org/10.1016/j.jnucmat.2020.152688
0022-3115/

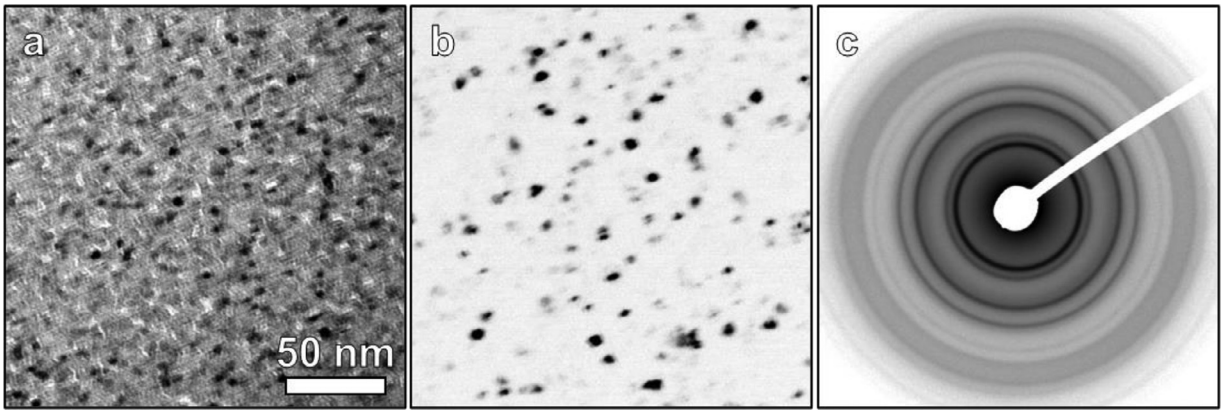

Fig. 1. The as-deposited CeO_2 microstructure as observed by TEM (a) bright-field, (b) dark-field, and (c) diffraction. The dark-field image was produced by placing the objective aperture around a portion of the first inner diffraction ring. The images show grains with diameters of a few nanometers. The dark-field image and diffraction pattern have inverted contrast for publication.

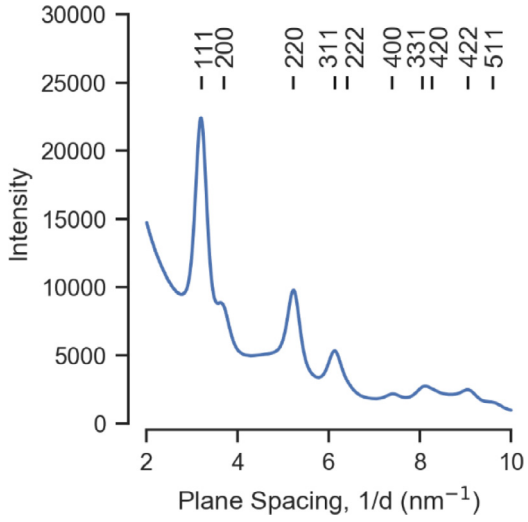

Fig. 2. Radial profile of the TEM diffraction pattern of CeO_2 obtained by an angular integration of the raw diffraction data. The expected locations of the diffraction peaks for the CeO_2 fluorite structure with a_0 = 0.541 nm are shown above the curve.

with carbon support films at ambient temperature. The CeO_2 thin film was approximately 50 nm thick. Post-deposition TEM characterization revealed equiaxed grains with an average size of 3.5 ± 0.3 nm, and the diffraction pattern was consistent with CeO_2 and showed no evidence of texture. Fig. 1 shows bright-field and dark-field images of the as-deposited grains, along with a diffraction pattern obtained. The dark-field image contrast is inverted for clarity. It should be noted that no preferential in-plane orientation is observed. The diffraction pattern was integrated around the circle to obtain the intensity versus plane spacing plot shown in Fig. 2. The pattern can be well indexed using the fluorite structure with a lattice parameter a_0 = 0.541 nm [17]. The sample thickness is an order of magnitude larger than the grain size, but the context of the thin-foil experiment with relatively high sample surface to volume ratio must remain under consideration.

2.2. In-situ irradiation

In-situ irradiation grain growth experiments were conducted at the Intermediate Voltage Electron Microscope (IVEM) facility at Argonne National Laboratory. The IVEM consists of a Hitachi 9000 TEM that is coupled to a NEC ion implanter to allow for simultaneous electron imaging and ion irradiation [18,19]. The irradiations were conducted using 1 MeV Kr^{2+} ions and a flux of 6.25 × 10^{15} ions/m^2s to maximum doses in the range of (1-3)x10^{19} ions/m^2. A heating holder allowed temperature control of the samples ranging from room temperature up to 1100 °C during irradiation. The sample temperature was measured by a thermocouple attached to the sample cup. The ion flux (and as a result the cumulative irradiation dose), the sample temperature, and sample microstructure were monitored continuously throughout the irradiation experiments. The irradiations were systematically paused at specific doses to readjust imaging conditions, record diffraction patterns, and to acquire high quality images.

The Stopping and Range of Ions in Matter (SRIM-2013) software was used to study the irradiation characteristics [20]. The "full cascade" option was chosen per the recommendation of Weber and Zhang [21]. A simulation of 25,000 1 MeV Kr ions was run for a 50 nm thick CeO_2 foil using displacement energies of 56 eV for cerium and 27 eV for oxygen [22–24]. Over 99% of the simulated ions transmitted completely through the sample. The simulation resulted in an average of 533 vacancies per ion which correlates to approximately 7.1 × 10^{18} ions/m^2 per displacement per atom (dpa). Therefore, the final ion doses reached in the in-situ irradiation experiments are on the order of a couple of dpa. Assuming surface binding energies of half the displacement energies, less than 2 nm sputtering is predicted.

2.3. Measuring grain size

During the grain growth experiments, the grain size was characterized by systematically acquiring dark-field TEM images as a function of increasing dose. This could be done either in a single region (so that individual grains could be monitored) or at various regions. The dark-field images were formed by inserting the objective aperture around a portion of the innermost CeO_2 diffraction ring which illuminated the subset of grains in that diffraction condition. Because of the sample inclination relative to the beam, a part of the sample was shadowed, as observed previously by Kaoumi et al. [25]. That provides an inherent control volume, which has undergone the same temperature history but no irradiation. Because there was no evidence for anisotropy of the grain structure in either the diffraction patterns or images, the subset of grains in the dark-field images was taken to be a representative sample of the whole.

The dark-field TEM images were then analyzed using an automated procedure to determine the grain size. The steps for this procedure were: (1) using Otsu's method [26] to threshold the im-

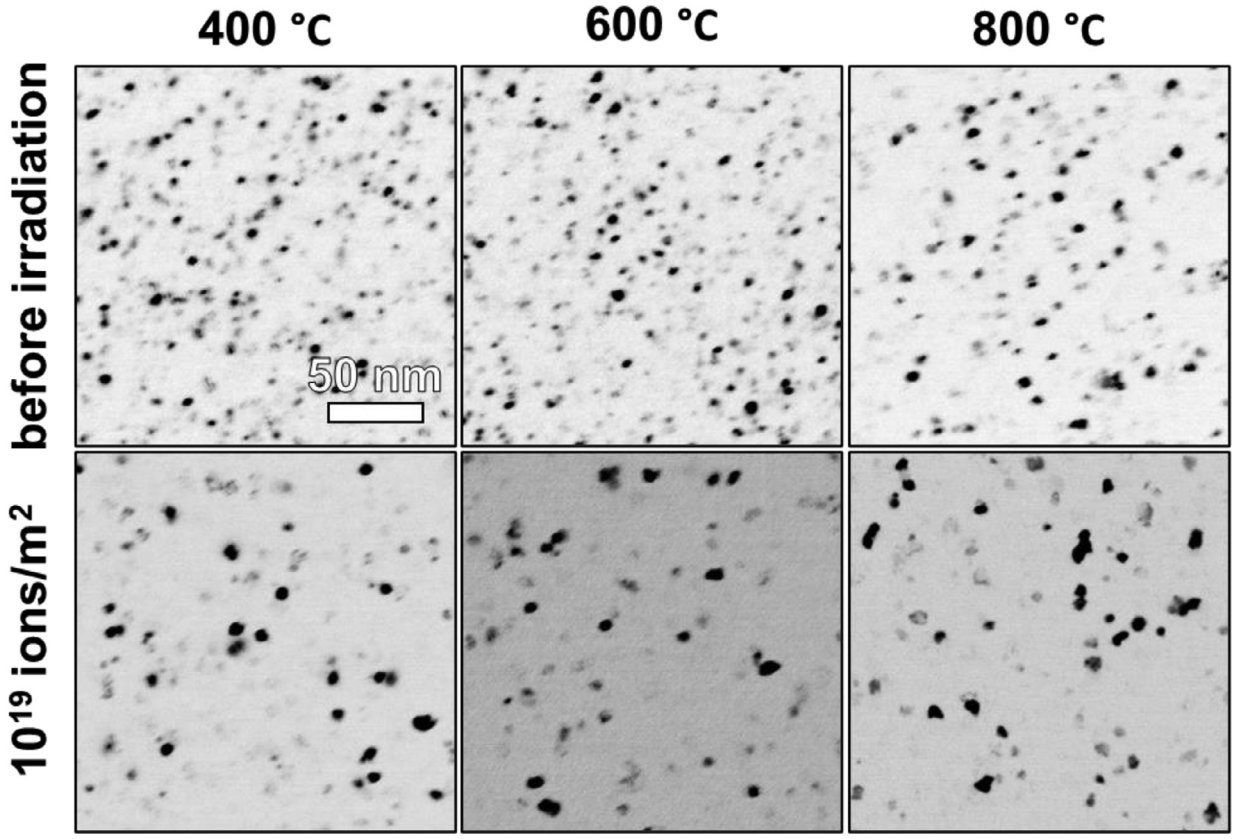

Fig. 3. Dark-field TEM images showing the grains in CeO_2 before and after independent in-situ irradiations to 10^{19} ions/m^2 at 400°C, 600°C, and 800°C. The grains grew from their as-deposited state, but the grain growth was only weakly dependent on irradiation temperature.

age and separate foreground and background, (2) fitting a two dimensional Gaussian function to the pixel intensity values of the background, (3) normalizing the original image to the fitted background Gaussian function,[‡] (4) re-thresholding the normalized image using Otsu's method, and (5) defining grains as the groups of foreground pixels connected by their sides or corners. The grain area measurements were converted to an effective diameter by assuming a circular shape. Grains with an effective diameter of less than 1 nm were discarded because of the microscope resolution. The average of all the remaining effective grain diameters is referred to as the average grain size. The error bars for the average grain size are calculated by error propagation of the pixel size (0.11 nm / pixel) and the standard error of the average grain size.

3. Results and Discussion

3.1. Irradiation of CeO_2 at 400°C, 600°C, and 800°C

Irradiating at 400°C, 600°C, and 800°C produced a gradual and monotonic increase in the average grain size. The grain growth mechanism appeared to be normal as no individual grains grew at a rate greatly exceeding the average. The average grain size increased by approximately 1 nm after irradiation to 10^{19} ions/m^2. The average grain size continued to increase with further irradiation, but the rate of grain growth decreased as the total irradiation dose increased. Fig. 3 shows dark-field images of the grains after irradiation to 10^{19} ions/m^2 at each irradiation temperature. Note that the contrast was reversed for clarity. These images show that the grain growth was not significantly affected by irradiation temperature up to 800°C.

Grain growth was not observed after heating the samples but before beginning irradiation. As mentioned above, a small part of the thin-films was shielded from the ion beam by the cup holder and in that region grain growth was not observed after the completion of the irradiation experiments, as shown in Fig. 4 and as also observed previously by Kaoumi et al. [25]. That is, the entire sample was subjected to the same thermal history, but only the area affected by the ion beam experienced grain growth. This indicates that ion irradiation was required for grain growth for the experiments conducted. The grain growth kinetics measured from sintering experiments [10,11] suggest that at 800°C, the maximum irradiation temperature used in this study, it would take thousands of hours to double the initial 3.5 nm grain size by the thermal mechanism alone.

The method outlined in Section 2.3 was used to measure grain growth in CeO_2. For each irradiation temperature one or more images were acquired at selected dose points and analyzed to determine the average grain size. The number of grains measured in each image ranged from approximately 100 to 500. This number of grains decreased as the grain size increased. Multiple data points for a single dose were acquired either from more than one location in the sample or from the same location but with dark-field images formed from a different portion of the diffraction ring to illuminate different grains. The results of the measurements are displayed in Fig. 5 where the average grain size is shown as a function of irradiation dose for each irradiation temperature. Grain sizes increased to nearly 6 nm for the maximum dose achieved.

Overall, the extent of grain growth observed during this work is less than that previously observed from 3 MeV Au^+ irradiation [12,13]. By comparing the doses achieved in each experiment

[‡] The dark-field images were acquired under non-parallel illumination. A Gaussian function was used to approximate the intensity profile of the convergent TEM beam and to flatten the image.

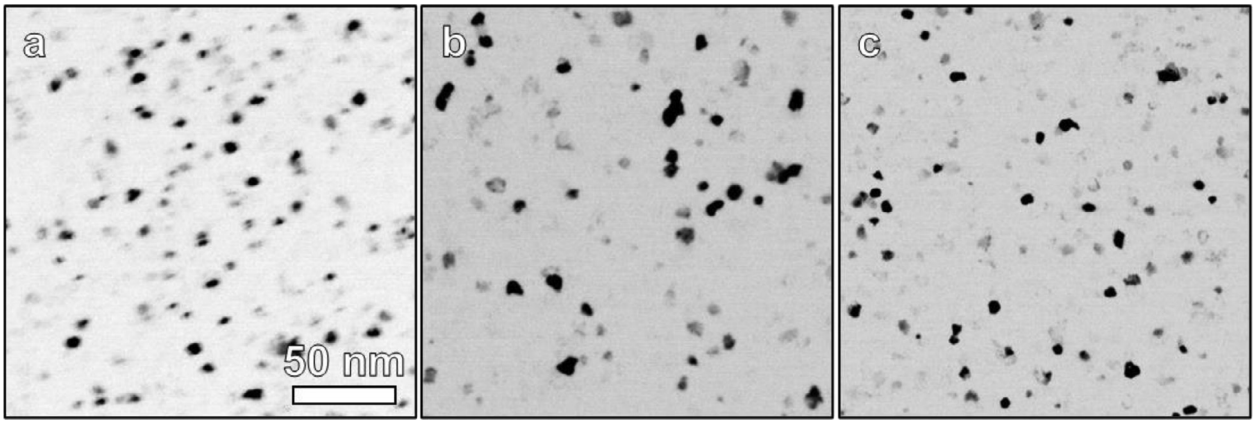

Fig. 4. A series of dark-field TEM images acquired during a single in-situ irradiation experiment of CeO_2 at 800°C (a) before irradiation, (b) after irradiation to 10^{19} ions/m^2, and (c) in a portion of the sample that was blocked from the ion beam. The grain size in the area where the ion beam did not hit is similar to that seen before irradiation.

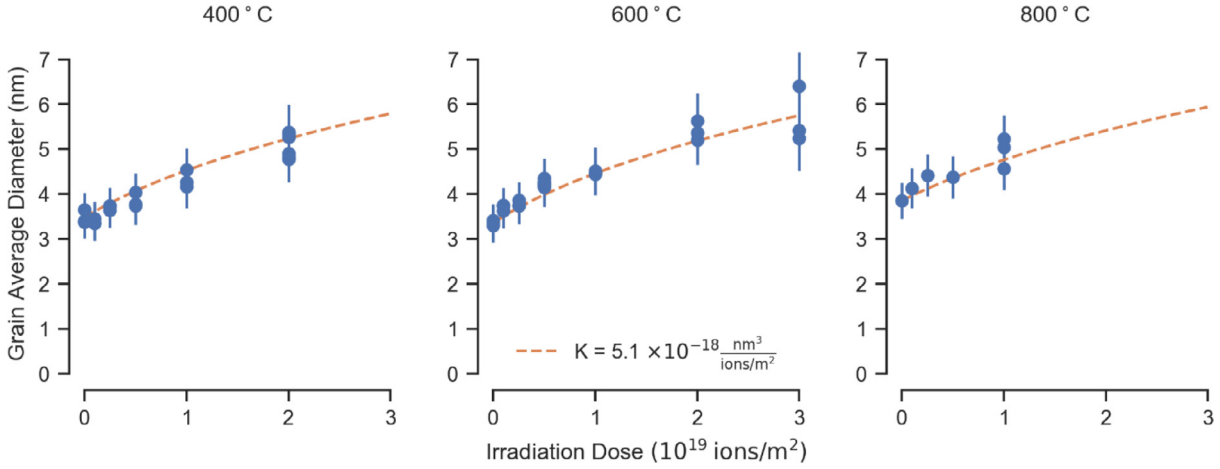

Fig. 5. The progress of CeO_2 grain growth with respect to irradiation dose for irradiations performed at 400°C, 600°C, and 800°C. Each point represents the data measured from a single image. Grain size increases with dose, and the line shows the best fit to the kinetics described by Eq. (2).

by units of dpa, the present work achieved an order-of-magnitude lower maximum dose than in that work, which logically results in less grain growth. The rate of grain growth per dpa is also lower in the present work, but the difference in ion species and energy makes a direct comparison difficult. However, in the current experiments grain growth was observed as a result of irradiation of ceria, in contrast to what was observed by Chang et al. [15].

3.2. Grain growth kinetics

Kaoumi et al. suggested that grain growth in metals under irradiation occurs as a result of thermal spikes induced by primary knock-on collisions [27]. The model assumes that as cascades hit a grain boundary, the atomic rearrangements in the resulting thermal spike are biased by the grain boundary curvature resulting in grain growth. A kinetic equation was derived using the number of atomic jumps across a grain boundary as the result of a thermal spike and driving force of the form

$$D^3 - D_0^3 = K\Phi t \tag{2}$$

where D_0 is the initial average grain diameter, D is the average grain diameter after time t, and Φ is the ion flux. The kinetic parameter K is defined as

$$K = 36\gamma d_{spikes}\chi\delta\frac{V_{at}\nu\sqrt{5/3}\Gamma(8/3)k_B^{5/3}Q^{5/3}}{10\pi C_0^{2/3}\kappa_0 E_a^{8/3}} \tag{3}$$

Table 1
The description and literature values of the variables needed to calculate the thermal spike grain growth kinetic parameter K for CeO_2.

Parameter	Variable	Value	Ref.
grain boundary surface energy	γ	1 J/m^2	[33]
thermal spike diameter	d_{spike}	8.8 nm	[27]
thermal spikes per ion	X	0.06 spikes/ion/nm	[20]
grain boundary width	δ	0.6 nm	[27]
atomic volume	V_{at}	0.0132 nm^{-3}	[17]
Debye frequency	ν	53.8 THz	[34]
Boltzmann constant	k_B	1.38 × 10^{-23} J/K	
average thermal spike energy	Q	19.8 keV	[20,27]
heat capacity	C_0	65 - 80 J/mol.K	[35]
thermal conductivity	k_0	7 W/m.K	[34]

where $\Gamma(8/3)$ is evaluation of the gamma function at 8/3, and E_a is the activation energy for atomic jumps. The remaining parameters are defined in Table 1, and their values listed.

The grain size measurements in this work were fit to Eq. (2) to determine an experimental value for K. The experiments showed that the irradiation temperature did not strongly affect the grain growth rate, and so a single value for K was determined by fitting to all of the data together. K was determined to be 51 nm^3/(10^{19} ions/m^2). Eq. (3) was rearranged to solve for the activation energy

for atomic jumps.

$$E_a = \left(36\gamma d_{spikes} \chi \delta \frac{V_{at} \nu \sqrt{5/3} \Gamma (8/3) k_B^{5/3} Q^{5/3}}{10\pi C_0^{2/3} \kappa_0 K} \right)^{3/8} \quad (4)$$

The activation energy was calculated using the experimental value of K and the other values listed in Table 1. The irradiation parameters Q, X, and d_{spike} were calculated using the SRIM simulation data and following the recipe by Kaoumi et al. [27]. Because the temperatures in the thermal spike are extraordinarily high, the heat capacity and thermal conductivity were chosen at the highest temperatures provided in the literature.

The results show that the three curves could be well fit using a single value of the parameter $K = 5.1 \times 10^{-18}$ nm^3/(ions/m^2). Using that value and the parameters in Table 1, the activation energy for thermal spike grain growth was calculated to be 8 eV. Experimentally determined values of the activation energy for *thermal* grain growth in pure CeO_2 from sintering experiments include 6.16 eV and 7.22 eV [10,11]. The activation energy determined in this work is larger than both of these literature values. However, there is uncertainty, especially within thermal spikes, of ceria material properties values such as the thermal conductivity, heat capacity, grain boundary energy, and Debye frequency. The activation energy calculated from this work would need to be reduced by 10% to 25% to match the literature values, which could be achieved by reasonable adjustment to one or a combination of parameters. Thus, the thermal spike model of grain growth originally applied to metallic systems may also apply to ceria. The thermal spike grain growth model can rationalize the observed irradiation grain growth in the context of irradiation parameters, but a better understanding of the temperature variation of ceria material properties and its effect on the model is needed.

Grain boundary mobility in ceria was attributed to the cation interstitial mechanism, and as a result grain boundary mobility increases with increasing oxygen vacancy concentration [28]. Experiments have shown that cerium in ceria can reduce from Ce^{4+} to Ce^{3+} at high temperatures under vacuum [29–31]. For ceria under vacuum, higher temperatures should therefore increase grain boundary mobility by increasing the thermal driving force and increasing the oxygen vacancy concentration relative to lower temperatures. In contrast to this logic, the irradiation experiments in this work showed that the irradiation temperature only weakly affected the grain growth rate. However, reduction of ceria by irradiation has also been reported [15,31,32]. The ceria in this study was irradiated at a dose rate of nearly 10^{-3} dpa/s, and on average each atom in the ceria was displaced more than once during each experiment. The ion irradiations produced large numbers of defects, including oxygen vacancies, which may have contributed to the grain boundary mobility and grain growth rate. The result that the irradiation temperature only weakly affected the grain growth rate, in absence of other variables, suggests that the irradiation itself strongly affected the grain growth rate. However, there are complex relationships between irradiation dose, dose rate, and temperature on defect density, and their effects on grain boundary mobility should be considered further.

4. Conclusion

Thin-film, nanocrystalline samples of CeO_2 were produced by EB-PVD onto TEM grids with a carbon film. The samples were individually irradiated in-situ at the IVEM using 1 MeV Kr ions to maximum doses up to (1 – 6) x10^{19} ions/m^2 at temperatures ranging from ambient room temperature to 800°C. The grain size was followed continuously in-situ in the TEM.

The ceria fluorite phase remained stable during irradiation at 400°C, 600°C, and 800°C, and irradiation induced grain growth occurred, as grain growth was not observed in the area of the sample shadowed from the ion beam. Little dependence on irradiation temperature was observed in the irradiation temperature range from 400°C to 800°C. Automated analysis was used to measure the grain size evolution as a function of dose. The results were analyzed using the thermal spike model, which rationalized that grain growth was weakly dependent on irradiation temperature, and the grain growth kinetics were fit well to a single equation.

Declaration of Competing Interest

The authors declare that they have no known competing financial interests or personal relationships that could have appeared to influence the work reported in this paper.

Acknowledgements

This work was funded by the U.S. Department of Energy's Nuclear Engineering University Program project number 17-12797. We would like to thank Tom Medill and Guy Showers of the Penn State Applied Research Laboratory for operating the CeO_2 deposition. We also thank the IVEM staff in general, and especially Pete Baldo for helping to perform the in-situ ion irradiation experiments.

References

[1] M. Zinkevich, D. Djurovic, F. Aldinger, Thermodynamic modelling of the cerium–oxygen system, Solid State Ion 177 (2006) 989–1001.
[2] C. Guéneau, M. Baichi, D. Labroche, C. Chatillon, B. Sundman, Thermodynamic assessment of the uranium–oxygen system, J. Nucl. Mater. 304 (2002) 161–175.
[3] T.L. Markin, R.S. Street, E.C. Crouch, The uranium-cerium-oxygen ternary phase diagram, J. Inorg. Nucl. Chem. 32 (1970) 59–75.
[4] D.-J. Kim, Ionic Conductivities, Lattice Parameters, Ionic Conductivities, and Solubility Limits in Fluorite-Structure MO_2 Oxide [M = Hf^{4+}, Zr^{4+}, Ce^{4+}, Th^{4+}, U^{4+}] Solid Solutions, J. Am. Ceram. Soc. 72 (1989) 1415–1421.
[5] B. Ye, M.A. Kirk, W. Chen, A. Oaks, J. Rest, A. Yacout, J.F. Stubbins, TEM investigation of irradiation damage in single crystal CeO_2, J. Nucl. Mater. 414 (2011) 251–256.
[6] B. Ye, A. Oaks, M. Kirk, D. Yun, W.-Y. Chen, B. Holtzman, J.F. Stubbins, Irradiation effects in UO_2 and CeO_2, J. Nucl. Mater. 441 (2013) 525–529.
[7] M. Hillert, On the theory of normal and abnormal grain growth, Acta Metall 13 (1965) 227–238.
[8] D. Fan, S.P. Chen, L.-Q. Chen, Computer simulation of grain growth kinetics with solute drag, J. Mater. Res. 14 (1999) 1113–1123.
[9] R.M. German, Coarsening in Sintering: Grain Shape Distribution, Grain Size Distribution, and Grain Growth Kinetics in Solid-Pore Systems, Crit. Rev. Solid State Mater. Sci. 35 (2010) 263–305.
[10] P.-L. Chen, I.-W. Chen, Grain Growth in CeO_2: Dopant Effects, Defect Mechanism, and Solute Drag, J. Am. Ceram. Soc. 79 (1996) 1793–1800.
[11] T. Zhang, P. Hing, H. Huang, J. Kilner, Sintering and grain growth of CoO-doped CeO_2 ceramics, J. Eur. Ceram. Soc. 22 (2002) 27–34.
[12] Y. Zhang, P.D. Edmondson, T. Varga, S. Moll, F. Namavar, C. Lan, W.J. Weber, Structural modification of nanocrystalline ceria by ion beams, Phys. Chem. Chem. Phys. 13 (2011) 11946–11950.
[13] P.D. Edmondson, Y. Zhang, S. Moll, F. Namavar, W.J. Weber, Irradiation effects on microstructure change in nanocrystalline ceria – Phase, lattice stress, grain size and boundaries, Acta Mater 60 (2012) 5408–5416.
[14] Y. Zhang, D.S. Aidhy, T. Varga, S. Moll, P.D. Edmondson, F. Namavar, K. Jin, C.N. Ostrouchov, W.J. Weber, The effect of electronic energy loss on irradiation-induced grain growth in nanocrystalline oxides, Phys. Chem. Chem. Phys. 16 (2014) 8051–8059.
[15] Y. Chang, Y. Guo, M. Li, K. Wang, L. Lv, D. Liu, Effects of crystal quality, grain–size and oxygen vacancy of nanocrystalline CeO_2 films under 1.5 MeV Au ion irradiation, J. Nucl. Mater. 518 (2019) 41–47.
[16] J. Singh, D.E. Wolfe, Review Nano and macro-structured component fabrication by electron beam-physical vapor deposition (EB-PVD), J. Mater. Sci. 40 (2005) 1–26.
[17] M. Yashima, S. Kobayashi, T. Yasui, Crystal structure and the structural disorder of ceria from 40 to 1497°C, Solid State Ion 177 (2006) 211–215.
[18] C.W. Allen, L.L. Funk, E.A. Ryan, New Instrumentation in Argonne's HVEM-Tandem Facility: Expanded Capability for in Situ Ion Beam Studies, MRS Online Proc. Libr. Arch. 396 (1995).
[19] M. Li, M.A. Kirk, P.M. Baldo, E.A. Ryan, TEM with in situ Ion Irradiation of Nuclear Materials: The IVEM-Tandem User Facility, Microsc. Microanal. 21 (2015) 437–438.
[20] J.F. Ziegler, M.D. Ziegler, J.P. Biersack, SRIM – The stopping and range of ions in matter (2010), Nucl. Instrum. Methods Phys. Res. Sect. B Beam Interact. Mater. At. 268 (2010) 1818–1823.

[21] W.J. Weber, Y. Zhang, Predicting damage production in monoatomic and multi-elemental targets using stopping and range of ions in matter code: Challenges and recommendations, Curr. Opin. Solid State Mater. Sci. 23 (2019) 100757.
[22] A. Guglielmetti, A. Chartier, L.van Brutzel, J.-P. Crocombette, K. Yasuda, C. Meis, S. Matsumura, Atomistic simulation of point defects behavior in ceria, Nucl. Instrum. Methods Phys. Res. Sect. B Beam Interact. Mater. At. 266 (2008) 5120–5125.
[23] K. Yasunaga, K. Yasuda, S. Matsumura, T. Sonoda, Electron energy-dependent formation of dislocation loops in CeO_2, Nucl. Instrum. Methods Phys. Res. Sect. B Beam Interact. Mater. At. 266 (2008) 2877–2881.
[24] H.Y. Xiao, Y. Zhang, W.J. Weber, Ab initio molecular dynamics simulations of low-energy recoil events in ThO_2, CeO_2, and ZrO_2, Phys. Rev. B 86 (2012) 054109.
[25] D. Kaoumi, A.T. Motta, R.C. Birtcher, Influence of alloying elements on grain–growth in Zr(Fe) and Cu(Fe) thin-films under in situ ion-irradiation, J. Nucl. Mater. 382 (2008) 184–189.
[26] N. Otsu, A Threshold Selection Method from Gray-Level Histograms, IEEE Trans. Syst. Man. Cybern. 9 (1979) 62–66.
[27] D. Kaoumi, A.T. Motta, R.C. Birtcher, A thermal spike model of grain growth under irradiation, J. Appl. Phys. 104 (2008) 073525.
[28] P.-L. Chen, I.-W. Chen, Role of Defect Interaction in Boundary Mobility and Cation Diffusivity of CeO_2, J. Am. Ceram. Soc. 77 (1994) 2289–2297.
[29] F. Zhang, P. Wang, J. Koberstein, S. Khalid, S.-W. Chan, Cerium oxidation state in ceria nanoparticles studied with X-ray photoelectron spectroscopy and absorption near edge spectroscopy, Surf. Sci. 563 (2004) 74–82.
[30] W. Xiao, Q. Guo, E.G. Wang, Transformation of $CeO_2(111)$ to $Ce_2O_3(0001)$ films, Chem. Phys. Lett. 368 (2003) 527–531.
[31] K. Ohhara, N. Ishikawa, S. Sakai, Y. Matsumoto, O. Michikami, Y. Ohta, Oxygen defects created in CeO_2 irradiated with 200MeV Au ions, Nucl. Instrum. Methods Phys. Res. Sect. B Beam Interact. Mater. At. 267 (2009) 973–975.
[32] L. Qiu, F. Liu, L. Zhao, Y. Ma, J. Yao, Comparative XPS study of surface reduction for nanocrystalline and microcrystalline ceria powder, Appl. Surf. Sci. 252 (2006) 4931–4935.
[33] N. Zouvelou, X. Mantzouris, P. Nikolopoulos, Surface and grain-boundary energies as well as surface mass transport in polycrystalline CeO_2, Mater. Sci. Eng. A 495 (2008) 54–59.
[34] M. Khafizov, I.- W. Park, A. Chernatynskiy, L. He, J. Lin, J.J. Moore, D. Swank, T. Lillo, S.R. Phillpot, A. El - Azab, D.H. Hurley, D. Clarke, Thermal Conductivity in Nanocrystalline Ceria Thin Films, J. Am. Ceram. Soc. 97 (2014) 562–569.
[35] M. Ricken, J. Nölting, I. Riess, Specific heat and phase diagram of nonstoichiometric ceria (CeO_{2-x}), J. Solid State Chem. 54 (1984) 89–99.